Journal of Environmental Chemical Engineering 14 (2026) 123986

Contents lists available at ScienceDirect

Journal of Environmental Chemical Engineering

journal homepage: www.elsevier.com/locate/jece

Pressure-responsive nanofiltration for seawater desalination using sodium metasilicate sol-gel draw solution: Performance enhancement and silicate fouling mechanisms

Tayma Kazwini [a], Lilyan Alsaka [a], Yahia Aedan [a], Abdulmajeed Al Askar [a,e], Zhaohua He [a], Islam Md Rizwanul Fattah [a], Alaa H. Hawari [b], Maryam Al-Ejji [c], Adnan Alhathal Alanezi [d], Hossein Ali Khonakdar [f], Ali Altaee [a,*]

[a] Centre for Green Technology, School of Civil and Environmental Engineering, The University of Technology Sydney, 15 Broadway, NSW 2007, Australia
[b] Department of Civil and Environmental Engineering, College of Engineering, Qatar University, P.O. Box 2713, Doha, Qatar
[c] Center for Advanced Materials, Qatar University, P.O. Box 2713, Doha, Qatar
[d] Department of Chemical Engineering Technology College of Technological StudiesThe Public Authority for Applied Education and Training (PAAET)P.O. Box 117, Sabah Al Salem, 44010, Kuwait
[e] Department of Chemical Engineering, College of Engineering and Computer Sciences, Jazan University, Jazan, Saudi Arabia
[f] Department of Polymer Processing, Iran Polymer and Petrochemical Institute, Tehran, Iran

ARTICLE INFO

Keywords:
Forward osmosis
Nanofiltration
Pressure-responsive
Membrane
Sol-gel

ABSTRACT

The forward osmosis (FO) process for seawater desalination by sodium metasilicate (SMS) sol-gel draw solution faces challenges due to the high cost of cellulose triacetate (CTA), low water flux, and high costs. To address this issue, a cost-effective membrane of high water permeability and salt rejection is required. Pressure-responsive nanofiltration (PRNF) membranes present an opportunity for enhanced FO performance due to their superior water permeability and fouling resistance. This study evaluated the PRNF membranes against the CTA benchmark, measuring water flux, recovery, rejection rate, and reverse salt flux (RSF) across hydraulic pressures of 0–4 bar using DI water, NaCl, and seawater feeds with a 1 M SMS draw solution. PRNF outperformed CTA, demonstrating an increased water flux at 4 bar, reaching 40 LMH and 12.34 LMH in the PRNF and CTA for DI water feed, but decreased to 7.09 LMH and 4.46 LMH for the same membranes with SW feed. The rejection rate of Si and Na ions was comparable in both membranes, exceeding 99%. Membrane fouling was identified because of irreversible Mg/Ca silicate scaling. Then, the performance of PRNF was investigated at 4 bar with SW in five consecutive filtration cycles, and EDTA was added to the feed to prevent Ca/Mg silicate fouling. Using NaOH at pH 11 for membrane cleaning between cycles minimised Mg/Ca silicate fouling on the active layer while eliminating such fouling in the support layer. The investigation found that at pH 9, silica polymerization-initiated fouling while Mg crosslinking stabilized the gel, whereas at pH 11, fouling is triggered by Ca-induced silica scaling. Additional, cross-sectional SEM of the PRNF membrane did not detect severe fouling or pore blockages, while the EDX mapping indicated weakly localised depositions of inorganic salts. XRD analysis further showed minor crystalline deposits on the active layer, mainly associated with calcite ($CaCO_3$) and possible brucite ($Mg(OH)_2$), while the support layer had even weaker crystalline deposits. Overall, compared with the CTA membrane, the PRNF membrane exhibited better water flux and solute retention.

1. Introduction

Forward osmosis (FO) has emerged as a promising alternative to reverse osmosis (RO) and nanofiltration (NF) for seawater desalination and wastewater treatment [1,2]. The overall performance of FO systems is strongly dependent on the membrane characteristics and draw solution properties [3,4]. High membrane permselectivity and a low structure parameter (S) are desirable for minimizing reverse salt flux (RSF) and internal concentration polarization (ICP), which are among the main limiting factors in FO performance [5,6]. However, the high cost of

* Corresponding author.
E-mail address: ali.altaee@uts.edu.au (A. Altaee).

https://doi.org/10.1016/j.jece.2026.123986
Received 16 May 2026; Received in revised form 21 June 2026; Accepted 5 July 2026
Available online 6 July 2026

FO membranes and their relatively low water flux are among other factors that continue to challenge the large-scale implementation of the FO technology [7,8].

Pressure-assisted forward osmosis (PAFO) uses hydraulic pressure on the feed side of the FO cell. Both the osmotic driving force of the draw solution and the hydraulic pressure are used to enhance the water flux and the recovery [9]. Kim et al. [10] investigated PAFO for CTA and NF90 membranes under applied hydraulic pressure on the feed. For the draw solution 0.9 M NaCl, the NF90 membrane had low RSF values measured at 2.5 and 5 bar, resulting in a J_s under 0.015 molMH, while the CTA membrane J_s values were more stable, approximately 0.1 molMH [10]. Another study by Jamil et al. [11] used PAFO for the treatment of reverse osmosis concentrate (ROC), applying hydraulic pressure of 2 and 4 bars to the feed. With 0.25 M potassium chloride (KCl) as the draw solution, water permeability increased by 9% at 2 bar and 29% at 4 bar [11].

Recent literature has explored stimuli-responsive methods as a phenomenon where external stimuli, such as physical (temperature), chemical (pH), or biological (bacteria) stimuli, cause physicochemical changes, including pore size and permeation flux [12]. Ou et al. [13] investigated nine combinations of thermo-sensitive N-isopropylacrylamide (PNIPAM) polyelectrolyte with sodium acrylate (SA) concentrations (ranging from 2% to 50%) as a draw solution in FO. The uniqueness of the polyelectrolyte is the lower critical solution temperature (LCST), which occurs at a temperature higher than 32 °C and produces a phase transition from hydrophilic to hydrophobic, releasing absorbed water without having to use excessive energy for heating. The study found that with an increase in SA, the LCST was not as effective and lost 50% of its LCST phenomenon [13]. Zeng et al. [14] developed a multi-layer temperature-responsive hydrogel based on poly(*N*-isopropylacrylamide-co-sodium acrylate) (P(NIPAAm-co-SA) for seawater desalination by the FO process. The study found that the combination of NIPAAm with sodium acrylate with a releasing layer is able to maintain the LCST of-35°C without compromising the dewatering mechanism of the polymer, and its drawing layer is responsible for the water flux. The maximum achieved water flux equated to approximately 0.29 LMH with NaCl as the feed solution, releasing 60% of the absorbed water in 60 min [14].

Applying pressure-responsive NF (PRNF) membranes in the FO process has recently been developed and applied as a novel approach to combine osmotic and hydraulic driving forces to accelerate water flux in high-permeability and selectivity NF membranes of a comparable design to the FO membranes [15]. Using conventional cellulose triacetate membranes (CTA) is well established, yet they achieve low water fluxes and have higher costs associated with them [16]. In the PRNF process, applying a small hydraulic pressure to the feed side of the membrane leads to a linear increase in the water flux, without compromising the membrane selectivity.

Khanafer et al. [15] applied a patented FO process [17] using pressure-responsive NF (PRNF) at 0, 2, and 4 bar, with TS80, XN45, and UA60 NF membranes. Using tertiary treated wastewater (TSE) as feed and thermal-plant brine as draw, the TS80 achieved a 99.6% rejection of divalent ions and linear water flux increase as the hydraulic pressure on the feed side of the membrane was adjusted from 0 bar to 2 bar to 4 bar, achieving 1.7 and 5.3-times greater water flux when the applied pressure reached 2 and 4 bar [15]. In another study, Khanafer et al. [18] compared the performance of the PRNF TS80 membrane (water permeability coefficient 8.63 LMH.bar) with Porifera TFC (water permeability coefficient 2.1 LMH.bar) and FTSH_2O (water permeability coefficient 0.69 LMH.bar) CTA FO membranes using 0, 2, and 4 bar hydraulic pressures [18]. The TS80 average water flux results increased linearly from 4.4 LMH at 0 bar to 13.8 LMH at 2 bar and reached 16.7 LMH at 4 bar. In comparison, the CTA FTSH_2O average flux was 5.7 LMH at 0 bar, 6.4 LMH at 2 bar, and 6.8 LMH at 4 bar, highlighting the significance of the hydraulic pressure on the permeation flux in the PRNF membranes. Aedan et al. [21] compared the performance of PRNF TS80 with FTSH_2O CTA at 0, 2 and 4 bar for PFOA-contaminated wastewater treatment by seawater draw solution. With a corresponding hydraulic pressure of 4 bar, the average water flux for the PRNF membrane was 42.87 LMH, with a 90% recovery rate reached in 6 h. In contrast, the CTA membrane had a water flux of 11.82 LMH, and it took 41 h to achieve the same 90% recovery rate. PFOA rejection rates are 99.1% with the PRNF membrane and 96.1% with the CTA [19]. Furthermore, the PRNF TS80 membrane demonstrated a consistent average water flux in multiple filtration cycles, recording 39.53 LMH, 38.4 LMH, and 37.75 LMH for the 1st, 2nd, and 3rd cycles.

There are a few studies about the application of PRNF membranes in the FO process for seawater desalination using a sol-gel draw solution. Sodium metasilicate (SMS) sol-gel was proposed as a draw solution due to its high osmotic pressure and no requirements for regeneration [20,21]. The sol-gel can be used for water and nutrient supply, nitrogen and phosphorus compounds, for plants when reacted with nitric or phosphoric acid:

$$Na_2SiO_3 + 2HNO_3 + H_2O \rightarrow H_4SiO_4 \downarrow + 2NaNO_3 \quad (1)$$

$$Na_2SiO_3 + H_3PO_4 + H_2O \rightarrow H_4SiO_4 \downarrow + 2NaH_2PO_4 \quad (2)$$

.

Silicic acid (H_4SiO_4) sol-gel is essential to boost the plant's immune system [22], while sodium nitrate or sodium dihydrogen phosphate are sources for nitrogen and phosphorus. Therefore, this study investigated the SMS sol-gel draw solution in pressure-responsive (PR) conditions. The use of SMS sol-gel, characterized by its high viscosity (5984 mPa.s) and pH-responsive polymerization behaviour [23], has not been studied with the PRNF membranes. Additionally, the SMS sol-gel is pH dependent, and silica polymerisation alters depending on the nitric acid concentration used, posing an increase in inorganic fouling, particularly focusing on silica scaling. In this study, a PRNF TS80 membrane was investigated for seawater desalination by a sol-gel draw solution, and the results are compared with the commercial FTSH_2O CTA membrane. The concept of PRNF applications in the FO process has been explored for seawater softening in thermal desalination and for treating wastewater contaminated with PFAS compounds. These applications have shown excellent performance when compared to conventional CTA FO membranes [15,24]. Previous studies have utilized traditional draw solutions like seawater, NaCl, and $MgCl_2$, but none have investigated the effect of a sol-gel draw solution on PRNF membranes. Three different feed solutions, i.e., DI water, NaCl, and seawater, as well as three different pressure applications, 0, 2, and 4 bar, were used to compare both membranes. The aim of this study includes: i) to evaluate the water flux and rejection rate of the PRNF membrane under various operating pressures and feed solutions, ii) to assess the PRNF membrane water flux and multiple filtration cycles, and iii) to investigate the impact of the draw solution pH on the PRNF membrane fouling and mitigation feasibility. Three feed solutions, i.e., DI water, 0.5 M NaCl, and seawater (SW), were studied with sodium metasilicate sol-gel draw solution in the FO system. Water flux decline was calculated in five consecutive filtration cycles using the PRNF TS80 membrane at 4 bar hydraulic pressure on the feed.

2. Materials and methods

2.1. Feed and draw solutions

Three feed solutions, DI water, 0.5 M NaCl, and real seawater, were utilized for both CTA and NF membranes. The seawater was pre-filtered using a 0.45 μm Durapore Membrane filter, obtained from Sigma-Aldrich, Australia, prior to use. The draw solution used was 1 M of sodium metasilicate (SMS), purchased from Sigma-Aldrich (Australia), combined with 70% concentration nitric acid (HNO_3) for pH adjustment. The pH of the SMS draw solution was adjusted to around pH 7, 9, or 11 using HNO_3 (Eq. 1). In this study, 300 mL of DI water was mixed

with 61 g of sodium metasilicate in a 1 L beaker under continuous stirring to make a homogeneous solution of 1 M concentration. The reaction was conducted in a fume hood, and nitric acid was gradually added to the SMS solution to adjust the solution pH to the desired level. Once silica gel started forming below pH 11, the additional 200 mL of DI water was added for a total of 500 mL DI water solution. Continuous mixing was maintained to stabilise the silica gel formation for up to 6 h, depending on the pH required. The pH of both the feed and draw solutions was measured using the calibrated Jenco (Australia) Vision Plus pH6810. The long-term performance of the PRNF TS80 membrane was carried out at 4 bar and evaluated in a five-filtration cycle of 6 h each. EDTA (7 g), purchased from Sigma-Aldrich (Australia), was mixed with 0.5 L of seawater feed solution under stirring to mitigate inorganic fouling by forming a stable metal-EDTA complex, as follows:

$$M^{2+} + EDTA^{4-} = [M\text{–}EDTA]^{2-} \quad (3)$$

.

Following each filtration cycle, the flat sheet membrane was rinsed with DI water and sodium hydroxide (NaOH) (Sigma-Aldrich, Australia), at pH 11 for 30 min.

2.2. Membrane and experimental setup

Two different types of flat sheet membranes were tested in the FO tests: the first was a cellulose triacetate membrane (CTA) FTSH_2O™ (Sterlitech Corporation, USA), with a contact angle of 68.1 ± 1 for the active layer and 60.2 ± 0.5 for the support layer, The second membrane used was a thin-film polyamide nanofiltration TS80 (TRISEP) membrane with a contact angle of 17.4 ± 1 for the active layer and 58.3 ± 0.5 for the support layer, which makes the TS80 more hydrophilic than the CTA. The pH range for the CTA is between pH 3–7, while for the TS80 it is 2–11, which allows the TS80 a greater range in the alkalinity pH. The membrane porosity of the pristine TS80 was 57% with a membrane thickness of 145 μm. The water permeability coefficient of the CTA FO membrane is 0.73 LMH.bar and 13.1 LMH.bar for the NF TS80 membrane [24]. The characteristics of the NF and CTA membranes are found in the Supplementary Materials (S1) [24,25]. A cross-flow Sterlitech CF042 bench-scale FO cell, with 42 cm^2 active membrane area, was used in all experiments (Sterlitech, USA).

Small hydraulic pressures of 2 and 4 were applied on the feed side of the PRNF membrane to stimulate the permeation flux in the PRNF membrane. Prior to each experiment, the membrane was placed within the FO cell and run with deionized water (DI water) for both the active and support layers of the membrane for approximately one hour for complete wetting. Using a WT3000–1JA Micro Gear Pump (Longer Pump) on each side, the solutions were circulated at 2 liters per minute (LPM) with a cross-flow velocity of 33 cm s^{-1}. There are two flow meters, type F−550 model (Blue White Industries Ltd), to record the flow rate of the solutions. As per Fig. 1, the feed solution is situated on top of an EK−15KL compact bench scale and connected to a laptop running the RsWeight software, recording the change in mass of the solution to calculate the water flux (Eq. 4):

$$J_w = \frac{\Delta m}{\rho A t} \quad (4)$$

Where Δm represents the difference in mass (kg), ρ represents the density of water (kg/L), A is the membrane area (m^2), and t represents time (h).

The Milwaukee MW306MAX portable meter was utilized to measure the conductivity of the feed solution that is required for calculating the reverse salt flux as per Eq. 5:

$$J_s = \frac{C_1 m_1 - C_0 m_0}{At} \quad (5)$$

.

J_s is the salt flux (g/m^2h), C_1m_1 is the feed concentration and mass after time (t), and C_0m_0 is the feed concentration and mass at time (0).

Eq. 6 was used to calculate the rejection rate, specifically for sodium (Na) and silicon (Si) levels present when DI water is the feed solution and sodium (Na) when NaCl is used as the feed solution:

$$R = \left(1 - \frac{C_p}{C_f}\right) \times 100\% \quad (6)$$

.

C_p (mg/L) is the permeate concentration, and C_f (mg/L) is the solute concentration.

The recovery rate, as per Eq. 7, is the ratio of permeate flow rate to the feed flow rate:

$$Recovery = \frac{Q_p}{Q_f} * 100\% \quad (7)$$

Where Q_p represents the permeate flow (m^3/h), and Q_f represents the feed flow rate (m^3/h). Furthermore, the common resistance-in-series model works under the assumption of a solid cake layer and constant pressure, limiting its effectiveness in detaching fouling components

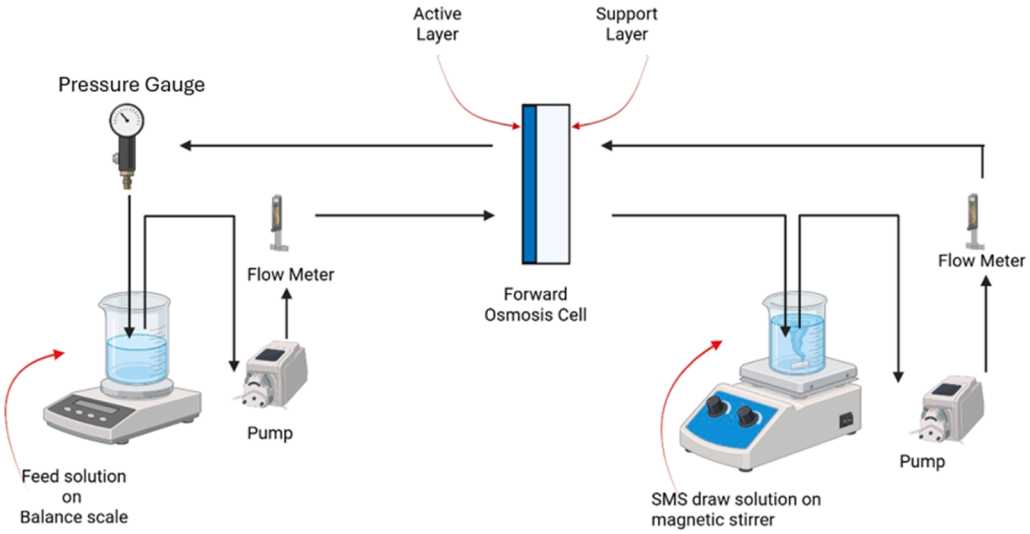

Fig. 1. Schematic diagram of the forward osmosis setup used in the sol-gel desalination experiments.

correctly in a sol-gel environment that responds to dynamic pressure fluctuations. In order to consider long-term water flux recovery, this study measured the total decline in water flux following chemical cleaning, highlighting the practical aspects of membrane cleaning efficiency and its potential reuse from an engineering standpoint.

It is noteworthy that the results reported in this study are reproducible and backed by an analysis of error variability, thorough characterization, and alignment with existing literature. Each experiment was replicated at least 3 times, and the results are presented as mean values. The Analysis of Variance (ANOVA) was employed to assess variations among multiple experimental data sets. Single-factor ANOVA, Two-Factor ANOVA Without Replication, and t-Test: Two-Sample Assuming Unequal Variances analysis for experimental data showed a P-value less than 0.05, indicating statistically significant differences between treatment groups.

3. Results & discussion

3.1. Sol-gel characterization

The SMS sol-gel was tested under pH 7, 8, 9, and 11 to systematically investigate the effects of varying pH levels on the conductivity, density, and FTIR. The SMS sol-gel is ultimately dependent on temperature and pH [20].

The density was calculated using a 25 mL volumetric flask at 23 °C. The flask was weighed empty with the stopper. Each SMS sample at a specific pH was weighed again when the SMS sol-gel was placed in it at different pH levels. Three readings were consistently taken for each pH level to obtain an average mass, and then the final density was calculated. Fig. 2a shows the density against the pH. The SMS sol-gel became slightly denser with alkalinity increase from pH 8–11 (0.48%) and has a consistent composition, indicating that any water flux changes will not be from density changes. In terms of the SMS sol-gel conductivity, it was 36.7 ± 0.2 mS/cm at pH 14, prior to any addition of nitric acid. As the pH of the solution increased from 8 to 11, the conductivity slightly decreased from 43.9 to 40.7 mS/cm, as shown in Fig. 2a. These changes are consistent with pH-driven alterations found in different types of silicates and ionic compositions. As the alkalinity increases, the silanol functional groups become more deprotonated and are likely to bond with free ions such as sodium.

SMS sol-gel samples underwent Fourier Transform Infrared (FTIR) analysis. Each sample was placed in a centrifuge for 10 min at 5000 RPM. The hydrogel was then placed in a 105 °C oven for 24 h to form a powder before the FTIR analysis (Fig. 2b). All samples have peaks in the range of 462–547 cm^{-1}, which fall within the Si-O-Si bending region. Samples at pH 7, 8, and 9 have peaks ranging from 794 to 813 cm^{-1}, aligning with Si-O-Si symmetric stretching and 1055–1138 cm^{-1} ranges aligning in the fingerprint region of Si-O-Si stretching. The results align with Bergna's. [26] investigation, where strong Si-O bands are observed within the ranges of 800 cm^{-1} and 1100 cm^{-1} across silica forms [26]. At 1344–1367 cm^{-1}, which is associated with pH 8 and 9, there is the peak ionization system where many reactions can effectively take place as the silicates remain unstable and are still reacting with other ions, as well as strong S═O stretching sulfonate groups. Samples at pH 9 and 11 have slight peaks at 3711 cm^{-1} and 3745 cm^{-1} associated with hydroxyl functional groups. Bergna's. [26] study attributed this to an isolated silanol group at 3750 cm^{-1}, suggesting the commencement of the deprotonation of the silicate ions. Additionally, a peak at 1523 cm^{-1} for the pH 11 sample shows N-O stretching groups, which can be related to nitric acid that has not yet fully bonded with the silicate ions.

Overall, the combination of density increase, a slight conductivity decrease, and pH-dependent changes in the Si-O-Si as well as O-H regions in FTIR analysis suggests that the increasing pH mainly influences silicate bonding environments and ion mobility within the SMS sol-gel. This finding is crucial in understanding the behaviour of the draw solution's ability to transport, as well as the effect of the osmotic behaviour across pH changes.

3.2. Water flux

3.2.1. DI water and NaCl draw solutions

Several FO tests were conducted to compare the pattern of water flux in correspondence to hydraulic pressures of 0, 2, and 4 bar for both the PRNF TS80 and the FTSH_2O CTA membranes, using three feed sources, i.e., DI water, 0.5 M NaCl, and seawater. Experiments investigated the impact of hydraulic pressure on the water flux of DI water to neutralize the effect of feed osmotic pressure and membrane fouling, 0.5 M NaCl, to underline the impact of the feed osmotic pressure on the water flux, and seawater, where membrane fouling is considered on the water flux. Experiments were conducted with the active membrane layer against the feed solution (ALFS) to guarantee the integrity of the PRNF TS80 membrane, which could be compromised when feed pressure is applied to the support membrane layer, leading to the delamination of its active layer [15,27]. All tests were conducted for a 6-hour duration at 1 M of SMS draw solution and a room temperature of 23 °C. To observe the pH tolerance of the membranes, the pH of the SMS sol-gel for the CTA membrane was maintained at circa pH 7, while for the NF membrane, the pH was kept at 11. These operational conditions align with the membranes' design specifications and adhere to the manufacturer's recommended guidelines and hence reflect the practical use of membranes in a real-life application. Sol-gel produced at pH 7, according to the Van't Hoff Equation (**section S4 of the** Supplementary Materials), has a slightly higher osmotic pressure (122.3 bar) than that prepared at pH 11 (97.8 bar), which will be in favour of water flux in the CTA. The greater osmotic pressure at pH 7 is brought about by the increased ionic strength due to the higher HNO_3 addition, thereby reducing ion pairing,

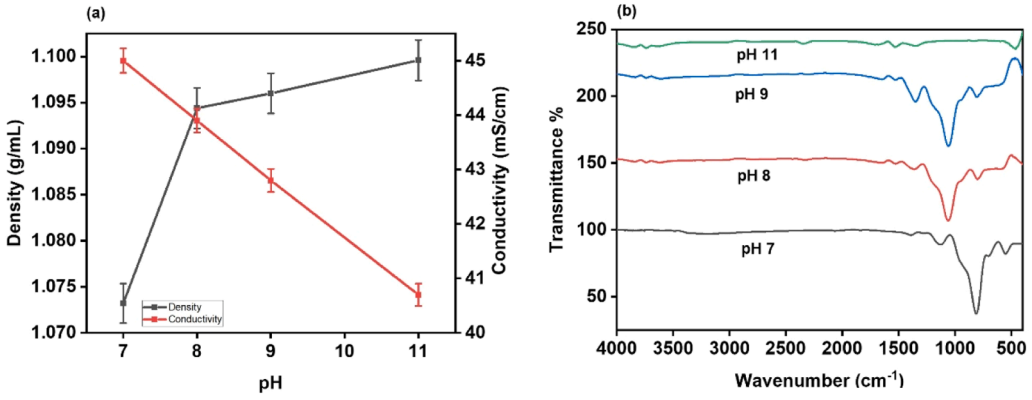

Fig. 2. a) conductivity and density vs. pH of SMS sol-gel, b) FTIR of SMS sol-gel at different pH levels. The error bar = 1 standard deviation.

larger availability of free Na and nitrate (NO_3^-) ions as silica stays partially polymerized.

Figs. 3a, 3b, and 3c depict the water flux in the PRNF TS80 and CTA FTSH_2O membranes at different feed solutions and pressures. In all experiments, the initial high water flux, followed by a sharp decline after 90 min, is an expected consequence due to the development of the fouling layer, concentration polarization (CP) within the membrane, as well as progressive dilution of the draw solution and the concentration of feed solutions in the case of 0.5 M NaCl and seawater tests. Additionally, membrane orientation is a critical factor influencing both ICP and membrane fouling in FO, particularly when comparing it to ALFS or ALDS orientations. In ALFS orientation, the feed solution and applied hydraulic pressure directly contact the dense active layer, helping minimize the penetration of foulants into the porous support layer and reducing internal pore blockage [28,29]. Therefore, fouling can occur as a surface deposition and ECP rather than internal fouling within the support layer. However, ALFS can intensify dilutive ICP within the support layer, which ultimately reduces the effective osmotic driving force and leads to flux decline during PRNF operation. [30].

Water flux was the largest at a 4-bar hydraulic pressure due to the combined hydraulic and osmotic pressure, leading to an enhancement of the driving force across the membrane. However, the PRNF membrane exhibited higher water flux corresponding to hydraulic pressures of 2 and 4 bar than the CTA due to its greater water permeability and hydrophilicity (Supplementary Materials S1).

In the DI water tests (Fig. 3a), the maximum water flux through the

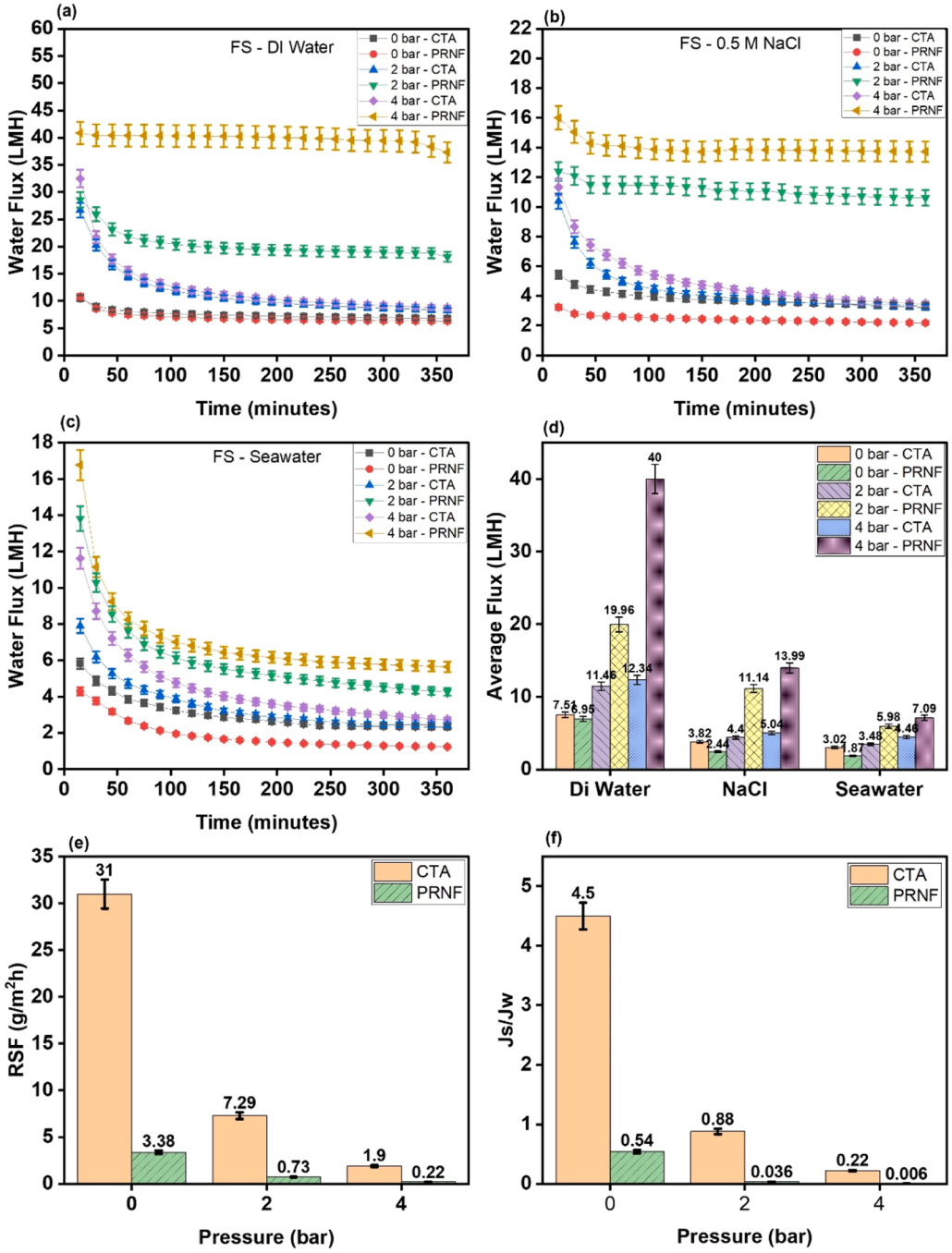

Fig. 3. Water flux comparing CTA and PRNF at 0, 2, and 4 bar for feed solutions: (a) DI Water, (b) 0.5 M NaCl, (c) seawater, (d) average flux of all experiments, (e) RSF of PRNF and CTA, (f) J_s/J_w membrane selectivity for PRNF and CTA membranes, DI water as feed. The error bar = 1 standard deviation.

CTA at hydraulic pressures of 0, 2, and 4 bar was measured at 10.7 LMH, 26.7 LMH, and 32.5 LMH, respectively. In contrast, the maximum water flux exhibited for the PRNF membrane corresponding to hydraulic pressures of 0, 2, and 4 bar was 10.8 LMH, 28.6 LMH, and 40.9 LMH. Interestingly, there was an intangible decline in water flux in the PRNF test conducted at 2 and 4 bar tests over time, indicating that DI water flux was largely driven by the hydraulic pressure and moderately affected by the dilution of the draw solution. The average water flux in the CTA membrane corresponding to hydraulic pressures of 0, 2, and 4 bar was 7.51 LMH, doubled to 11.46 LMH, and 12.34 LMH, whereas for the PRNF membrane, at hydraulic pressures of 0, 2, and 4 bar, resulted in 6.95 LMH, 19.96 LMH, and 40 LMH (Fig. 3d). Upon increasing the pressure from 2 to 4 bar, there is about an 8% and a 100% increase in the average water flux in the CTA and PRNF membranes. Due to the CTA membrane's limited water permeability coefficient (Supplementary Materials S1), it was found that the average flux had small increases.

When a 0.5 M NaCl feed solution is utilised, there is a clear reduction in the water flux compared to DI due to the attenuation in the osmotic driving force and CP phenomena (Fig. 3b). The maximum water flux in the CTA corresponding to hydraulic pressures of 0, 2, and 4 bar was 5.4 LMH, 10.4 LMH, and 11.3 LMH, while in the PRNF membrane, it was 3.2 LMH, 12.4 LMH, and 16.0 LMH at 0, 2, and 4 bar. At 0 bar, the inferior water flux in the PRNF membrane compared to the CTA is attributed to its high resistance, but water flux in the PNRF was stimulated by applying slight hydraulic pressure to the feed. The PRNF membrane is an NF membrane featuring a dense active layer that can endure high operating pressures. At 0 bar, the dense layer creates significant resistance to the osmotic flow, whereas the CTA membrane is a specially designed FO membrane aimed at reducing CP and achieving a higher baseline water flux. The PRNF membrane exhibited a stable water flux over time in the 4-bar test and, to a lesser extent, in the 2-bar test, due to membrane permeability and negligible fouling. At the end of the experiments, the average water flux in the CTA membrane corresponding to hydraulic pressures of 0, 2, and 4 bar was 3.82, 4.40, and 5.04 LMH, revealing a marginal increase in average water flux compared to the PRNF membrane at 0, 2, and 4 bar, which was 2.44 LMH, 11.14 LMH, and 13.99 LMH (Fig. 3d). Changing the feed salinity from DI water to 0.5 M NaCl caused up to a 59.15% drop in the average water flux in the CTA and a 65% drop in the average water flux in the PRNF membrane due to the CP effects and a diminishing of the osmotic pressure across the membrane.

3.2.2. Seawater draw solution

As for seawater (Fig. 3c), the trend of water flux was different from that for the DI water, and 0.5 M NaCl feeds, particularly for the PRNF membrane, exhibiting a sharp drop in the water flux over time. This trend is attributed to the combination of increasing CP effects over time and membrane fouling by seawater, thus declining water flux in the FO. Sharp water decline in the seawater experiments was a consequence of membrane fouling combined with the CP effects, triggering a 66.7% decline in the water flux during the PRNF test at 4 bar, compared to 8.7% and 14.4% decline during the PRNF tests at DI water and 0.5 M NaCl feed solutions. The EDX results (Table 2a) show increased amounts of Ca, Mg, Si, Na, and S on the active layer and Ca, Si, Mg, and Na on the support layer, indicating their potential accountability for membrane fouling and water flux decline. In contrast, the dynamic dilution of the draw solution and the concentration of the feed solution are responsible for the decline in the water flux (Fig. 3c). Although the initial water flux started higher in the seawater tests, it declined rapidly in the CTA and PRNF membranes, reaching a lower level than that in the NaCl tests (Figs. 3b and 3c). For the CTA, the corresponding water flux to hydraulic pressures of 0, 2, and 4 bar was 5.8 LMH, 7.9 LMH, and 11.6 LMH, compared to the PRNF membrane, where water flux at hydraulic pressures of 0, 2, and 4 bar was 4.3 LMH, 13.8 LMH, and 16.8 LMH. The CTA membrane produced an average flux corresponding to hydraulic pressures of 0, 2, and 4 bar, which was 3.02 LMH, 3.48 LMH, and 4.46 LMH, respectively. In comparison to the PRNF membrane, for 0, 2, and 4 bar, water flux was 1.87 LMH, 5.98 LMH, and 7.09 LMH. At 4 bar, the average water flux in the CTA test with seawater was 88% of that in the 0.5 M NaCl tests. The corresponding average water flux in the PRNF with seawater feed was almost 50% of that achieved in the 0.5 M NaCl feed.

Due to the superior permeability of the PRNF membrane, the EDX results in Table 2a show the main fouling components on the support and active layers for the feed solutions of DI water, 0.5 M NaCl, and SW with sodium metasilicate sol-gel draw solution. In the active membrane layer, the silicon content of 0.76% and 6.38% detected in the DI water and NaCl feed tests resulted from silicate species back diffusion from the draw solution. The increased silicon content of 2.57%, 27.61%, and 32.7% for DI water, 0.5 M NaCl, and SW detected in the support layer resulted from intensive ICP and hindered back diffusion of the sol-gel species. Silicate species in the sol-gel draw solution polymerize at pH 9, constituting a three-dimensional network of siloxane bonds (Si–O–Si) that could be responsible for silica gel layer fouling in the active and support layers and water flux decline. The source of trace sodium content, 2.3% in the active layer and 0.72% in the support layer, in the DI water feed test, was the draw solution, while the source of 1.63% and 1.33% chloride content in the support layer was the NaCl and SW feed solutions. As for SW feed at pH 11, although silicate species remain soluble, mainly as orthosilicic acid and hydrogen silicate, fouling was triggered by localised depositions of calcite and brucite residue and some weak NaCl residue. In addition to that, there is a potential pathway of Ca-induced silicate scaling and amorphous Mg–silicate depositions. At the beginning, silicate species diffuse into the support layer from the draw solution, whereas Ca and Mg diffuse from the seawater feed, forming Ca–silicate scale, followed by Mg–silicate deposition within the membrane pores, as follows:

$$Ca^{2+} + SiO_3^{2-} \rightarrow CaSiO_3(s) \quad (8)$$

$$Mg^{2+} + SiO_3^{2-} \rightarrow MgSiO_3(s) \quad (9)$$

.

Magnesium and calcium silicate fouling will be anchored in the pores of the support layer, leading to a diminished water flux. The trace chloride in the support layer is from the SW feed solution. In all experiments, the reduction in carbon in the active and support layers is attributed to the foulant materials covering the membrane surface, compromising the membrane permeability over time. The findings of these experiments imply that higher water flux promotes the transport of fouling precursors to the membrane surface, although fouling intensity is primarily controlled by the RSF rather than flux alone. In addition to Mg and Ca-induced silica fouling, XRD (Fig. 4k) results indicate the formation of calcite ($CaCO_3$) deposits on the membrane surface caused by the highly alkaline environment of the draw solution across the membrane. Minor reflections also suggest possible Mg-based alkaline scaling, such as brucite ($Mg(OH)_2$), together with possible calcium silicate-related deposition. However, these deposits appear localised and do not indicate severe support layer pore blockage or membrane deterioration.

3.3. Reverse solute flux and rejection

The reverse solute flux (RSF) was investigated using a DI water feed solution to study the influence of applied hydraulic pressure on the back diffusion of solutes from the draw to the feed solution. In the FO process, the RSF is governed by the membrane's solute permeability (B) and the concentration gradient across the active layer; however, the osmotic gradient on the membrane surface is strongly altered and impacted by the ECP/ICP phenomena [31]. Under pressure-responsive operating conditions, increasing the applied feed pressure increases water flux,

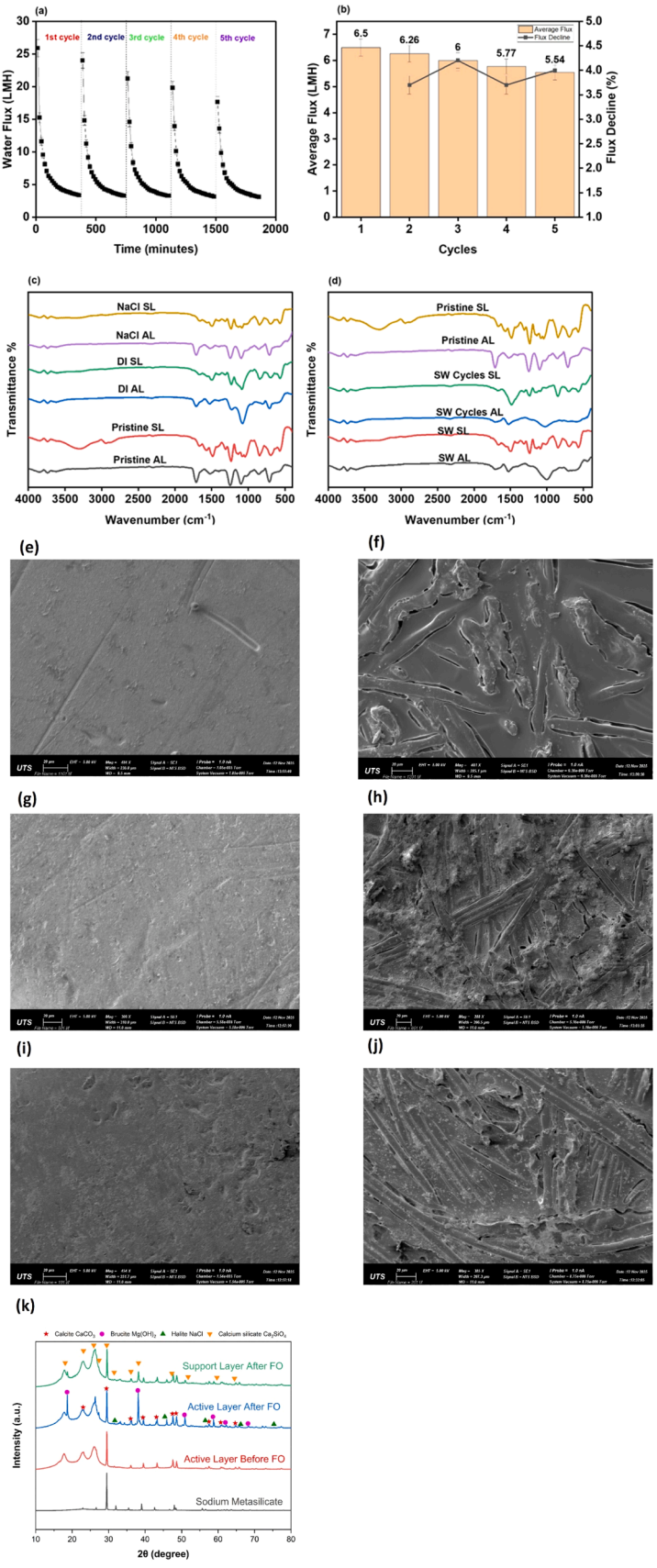

(caption on next page)

Fig. 4. (a) Water flux of PRNF cycles at pH 9, (b) Average flux and flux decline for each PRNF cycle at pH 9 (the error bar = 1 standard deviation) (c) FTIR of pristine NF membrane compared to active and support layers of feeds DI water and 0.5 M NaCl, (d) FTIR of single cycle SW active and support layer of PRNF at pH 11, compared to SW cycles at PRNF pH 9 against the pristine NF, (e) SEM image of active layer of pristine PRNF, (f) SEM image of support layer of pristine PRNF, (g) SEM image of active layer of single cycle of seawater PRNF at 4 bar pH 11, (h) SEM image of support layer of single cycle of seawater PRNF at 4 bar pH 11, (i) SEM image of active layer of seawater PRNF in 5 filtration cycles at 4 bar pH 9, (j) SEM image of support layer of seawater PRNF in 5 filtration cycles at 4 bar pH 9, (k) XRD patterns of the membrane before and after seawater PRNF in 5 filtration cycles at 4 bar at pH 9 SMS sol-gel draw solution, compared with SMS powder and reference markers for calcite $CaCO_3$, brucite $Mg(OH)_2$, halite NaCl, and calcium silicate Ca_2SiO_4.

which intensifies dilutive ICP on the SMS sol-gel draw solution side. As the sol-gel will become more diluted, the concentration of ions at the boundary layer of the draw solution decreases, leading to a decline in the RSF. This finding is in agreement with the literature, which demonstrated that the increase in the water flux contributes to the dilution of boundary layer ions and reduces the RSF [32]. As observed from Fig. 3e, this behaviour was most pronounced for the PRNF TS80 membrane as RSF declined significantly from 3.38 g m^{-2} h^{-1} at 0 bar to 0.73 g m^{-2} h^{-1} at 2 bar and reached 0.22 g m^{-2} h^{-1} at 4 bar. Fig. 3e shows an approximate 78% reduction in the RSF as the feed pressure rose from 0 to 2 bar, and more than 70% reduction as the pressure rose from 2 to 4 bar. Corresponding with the RSF decline, membrane selectivity (J_s/J_w) was improved from 0.54 g/L at 0 bar, 0.036 g/L at 2 bar, and reached 0.006 g/L at 4 bar. As such, increasing the feed pressure enabled advantageous improvements in water flux, reduced the RSF, and enhanced the membrane selectivity.

In contrast, the CTA membrane recorded 58.97 g m^{-2} h^{-1} RSF at 0 bar, greater than the PRNF membrane, and dramatically reduced to 7.29 g m^{-2} h^{-1} at 2 bar, and further reduced by 74% to 1.9 g m^{-2} h^{-1} at 4 bar. The corresponding J_s/J_w values for the CTA were 8.7 g/L at 0 bar, 0.88 g/L at 2 bar, and 0.22 g/L at 4 bar, indicating that due to CTA's lower selectivity in comparison to the PRNF's selectivity, is resulting to its weaker electrostatic exclusion and its higher structural resistance for mass transfer. Overall, the PRNF membrane demonstrated a lower RSF than the CTA due to the higher water flux that diluted the concentration of ions in the boundary layer of the draw solution and its stronger electrostatic repulsion to ions due to its higher negative charge (S1).

Table 1 shows the rejection trends for CTA and PRNF at 0, 2, and 4 bar hydraulic pressures and feed solutions of DI water and 0.5 M NaCl. In the experiment with the DI water feed solution, the back diffusion of Na and Si ions was measured by the ICP-MS, while in the 0.5 M NaCl feed solution, resembling seawater osmotic pressure, the Si concentration was only measured since Na is omnipresent in the feed and draw solutions. For DI water tests, more than 99% Na rejection was achieved for both membranes at 0 bar. The CTA membrane demonstrated a consistent sodium rejection of 99.12% at 0 bar, 99.25% at 2 bar, and 99.36% at 4 bar, exhibiting only minor increases with varying hydraulic pressures. The PRNF TS80 membrane exhibited a slightly higher rejection of Na than the CTA and was more consistent, at 99.53 ± 0.05%, 99.54 ± 0.05%, and 99.55 ± 0.05% at 0, 2, and 4 bar. Notably, the diffusion of ions in the membrane is controlled by the concentration gradients across the membrane. The slight increase in Na rejection was probably caused by the higher water flux that affected the concentration of the draw solution, hence the ion diffusion.

Table 1
Rejection percentage of Na and Si ions for PRNF and CTA membranes for DI water and 0.5 M NaCl feed solution, and 1 M SMS sol-gel.

		0 bar		2 bar		4 bar	
	Feed	Na (%)	Si (%)	Na (%)	Si (%)	Na (%)	Si (%)
PRNF	DI water	99.53 ± 0.05	98.99 ± 0.05	99.54 ± 0.05	99.33 ± 0.05	99.55 ± 0.05	99.36 ± 0.05
CTA	DI water	99.12 ± 0.05	99.1 ± 0.05	99.25 ± 0.05	99.27 ± 0.05	99.36 ± 0.05	99.4 ± 0.05
PRNF	NaCl	-	95.87 ± 0.05	-	99.29 ± 0.05	-	99.32 ± 0.05
CTA	NaCl	-	99.28 ± 0.05	-	99.4 ± 0.05	-	99.43 ± 0.05

Similarly, the Si rejection remained high and increased with pressure, especially for the CTA membrane. For the DI water tests, the CTA membrane rejected 99.1 ± 0.05% of Si ions at 0 bar, 99.27 ± 0.05% at 2 bar, and 99.4 ± 0.05% at 4 bar, while the PRNF rejected 98.99 ± 0.05% of Si at 0 bar, 99.33 ± 0.05% at 2 bar, and 99.36 ± 0.05% at 4 bar. However, when testing feed solutions with 0.5 M NaCl ionic concentrations, Si rejection for the CTA membrane remained almost constant, 99.28 ± 0.05% (0 bar), 99.4 ± 0.05% (2 bar), and 99.43 ± 0.05% (4 bar), while for the PRNF the Si rejection was slightly lower at 95.87 ± 0.05% at 0 bar, then increased to 99.29 ± 0.05% at 2 bar, and 99.32 ± 0.05% at 4 bar. Interestingly, slightly higher rejection of Si by the CTA compared to the PRNF at 0 bar hydraulic pressure was mainly caused by the lower water flux in the PRNF (Fig. 3b), keeping the concentration of the draw solution high and hence more Si ions diffused to the feed side. As pressure increased to 2 bar and 4 bar, the water flux of the PRNF membrane increased (Fig. 3b), diluting the concentration of the draw solution at the membrane surface while the Si diffusion dropped (Table 1). The results indicate that there was no correlation between the selectivity of the PRNF and CTA membranes and the PR application on the feed, whilst simultaneously achieving higher water flux. The PRNF's consistent increase in rejection with the increase in hydraulic pressure reveals that the PRNF membrane is able to not only reduce the solute transport under higher pressure but also mitigate back diffusion whilst increasing water flux.

3.4. PRNF cycles

Further experiments were conducted for the PRNF membrane consisting of 5 consecutive 6-hour cycles to evaluate membrane operational stability under repeated pressurised operation. All cycles were performed at a constant applied feed pressure of 4 bar with the membrane in ALFS orientation. Initially, the alkalinity of the draw solution was fixed at pH 11, but the FO tests demonstrated that sol-gel at pH 11 induced severe Mg/Ca-silicate scaling, causing a vast reduction in water flux of 42.98% and 32.31% in the filtration cycles 2 and 3 (Supplementary Materials S2). Thus, sol-gel was maintained at 1 M concentration while the pH was adjusted to pH 9 in the multiple filtration cycles to avoid the formation of Mg/Ca-silicate scaling. Seawater was used as the feed solution, and EDTA was introduced to chelate complex divalent ions, e.g., Ca^{2+} and Mg^{2+}, which were found to be critical for membrane fouling. Between filtration cycles, the flat sheet membrane was chemically cleaned using NaOH at pH 11 for 30 min on both sides of the membrane and then rinsed with DI water for 30 min.

Multiple filtration cycles revealed two different water flux patterns, with a steep drop in water flux at the first 60–90 min of the filtration cycle due to the reduced osmotic driving force and a slight reduction in initial water flux of consecutive cycles caused by the membrane's irreversible fouling. In the 1st cycle, the maximum water flux started at 25.9 LMH but diminished to 3.34 LMH after the 6-hour operation, corresponding to an 87.1% flux decline. Similar declines were observed in subsequent cycles, where for the 2nd cycle, the maximum water flux reached 24 LMH and decreased to 3.3 LMH, an 86% flux decline after 6 h. The 3rd cycle had a maximum flux of 21.2 LMH and decreased to 3.27 LMH, an 84.6% flux decline. The 4th cycle had a maximum flux of 19.8 LMH and decreased to 3.13 LMH, an 84.2% flux decline, while the 5th cycle had a maximum flux of 17.6 LMH and decreased to 3.09 LMH, an 82.5% flux decline. The drop in the water flux at the beginning of

filtration cycles is attributed to the irreversible membrane fouling. Fig. 4b shows the average flux and the flux decline for each cycle. After the 2nd cycle, there was a 3.7% flux decline, and after the 3rd cycle, there was a 4.2% flux decline. After the 4th cycle, there was a 3.7% flux decline, and after the 5th cycle, there was a 4% flux decline. Fig. 4b shows a 14.7% decline in the average water flux after five filtration cycles, while the flux decline in water flux remained almost stable, fluctuating between 3.7% and 4.2%. Notably, the maximum water flux for the 1st cycle (25.9 LMH) and the 5th cycle (17.6 LMH) had a 32% decline, which reflects the condition of the membrane surface at the time of contact, while the 14.7% decline in average water flux reflects the functional stability of the membrane and fouling layer resistance over time. As such, the average water flux should be the indicator used for the design of a full-scale plant.

3.5. SEM, EDX, XRD, FTIR

The EDX analysis reveals trace amounts of Mg, Ca, and Si on the active layer and Si and Mg, but minimal amounts of Ca on the support layer (Table 2b). EDTA chelates Mg and Ca in the SW feed, mitigating their diffusion to the draw solution side and the possible formation of calcium and magnesium silicate and/or carbonate deposits. From Table 2b, on the active layer side, the trace amount of Mg and Ca could be linked to the formation of EDTA complexes, while the trace amount of Ca on the support layer indicates insignificant transport from the SW feed side [33]. The lower Ca fouling on the active layer is attributed to its strong affinity to EDTA compared to Mg. The stability constant (K) for Ca is an order of magnitude larger than that of Mg, according to the Equations:

$$Ca^{2+} + EDTA^{4-} \rightarrow [Ca - EDTA]^{2-} \quad \log K \approx 10.7 \tag{10}$$

$$Mg^{2+} + EDTA^{4-} \rightarrow [Mg - EDTA]^{2-} \quad \log K \approx 8.7 \tag{11}$$

.

Additionally, the larger ionic radius of Ca (1.0 Å) fits well into the EDTA's hexadentate cage compared to Mg (0.72 Å). The higher charge density of Mg makes it more difficult to shed its hydration shell compared to Ca, which tends to lose its hydration shell easily. Table 2b also shows a trace of N on the active side that is likely from the Ca/Mg-EDTA complex adsorbed on the membrane surface. The lower C on the active and support layers after filtration is due to membrane surface masking by fouling materials. Compared to SW without EDTA tested at pH 11 (Table 2a), membrane fouling after five filtration cycles with EDTA tested at pH 9 (Table 2b) was less tenacious and more reversible than silica fouling in the absence of EDTA in the SW feed. Adding EDTA mitigated the severe internal silica fouling in the SW feed to adequate levels, with silicate content in the support layer reduced from 32.7% without EDTA to 8.5% with EDTA. The Ca and Mg fouling that occurred in the tests without EDTA was mitigated in the tests with multiple filtration cycles with EDTA, indicating the effectiveness of the fouling mitigation protocol. EDX analysis also revealed that Mg/Ca silicate deposits were localised on the support membrane layer, with silicon content on the selective membrane layer reduced from 8.84% to 2.7%, and on the support layer from 32.7% to 8.5%, indicating that membrane fouling became less intensive (Table 2a & 2b). Additionally, cross-sectional SEM was carried out for the 5 x PRNF cycles (in Supplementary Materials S6) and is consistent with the findings of the EDX in Table 2b.

XRD characterisation was used (Fig. 4k) to examine crystalline deposits formed on top of the membrane surface after the FO filtration cycles with SMS on the draw solution and seawater as the feed solution. For comparison, the XRD diffraction pattern of the pristine membrane before FO testing revealed peaks centred around 17.8°, 22.9°, 26.1°, 29.5° and 47.6°, corresponding to the membrane with some minor native instrumental background. After the FO test, the membrane retained the main membrane-related peaks at approximately 17.8°, 22.9°, 26.1°, 29.5°, and 47.6°, indicating that the membrane structure remained largely unchanged after the FO test. Furthermore, the membrane contained other crystalline material that produced reflections that were significantly higher in intensity and centred around 18.6°, 29.5°, 36.2°, 38.2°, 39.5°, 43.2°, 47.6°, 48.6°, 51.0°, 57.6°, 58.8°, 61.1° and 64.8°. Phase matching suggests that the crystalline material present on the membrane surface after FO filtration is primarily calcite ($CaCO_3$), as shown by its strong reflections near 29.5°, 36.2°, 39.5°, 43.2°, 47.6° and 48.6°, suggesting $CaCO_3$ scaling formed on the membrane surface after the FO test. Calcite formation can occur from high alkalinity conditions provided by the SMS draw solution, driving the carbonate equilibrium towards supersaturation of Ca^{2+} and CO_3^{2-} species at the membrane-solution interface. Minor peaks corresponding to possible Mg-based alkaline scaling species such as brucite ($Mg(OH)_2$) are noted around 18.6°, 38.2° and 51.0°.

The XRD phase matching also indicated possible calcium silicate-related reflections, supporting silicate-associated deposition as a possible pathway. The SMS powder used as a reference also showed XRD reflections centred around 22.9°, 29.5°, 32.0°, 39.1° and 48.1°, suggesting the presence of SMS residues or silicate scaling that may contribute to the XRD diffractogram following FO treatment. The support-layer XRD pattern showed weaker crystalline deposition than the active layer; however, weak calcium/silicate-related reflections suggest that silicate-associated deposition may occur within or near the support structure. Therefore, Ca/Mg–silicate interaction is discussed as a possible pathway contributing to flux resistance, rather than as a confirmed pore-anchoring mechanism. Further chemical surface studies are suggested in future work to verify the exact silicate-related bonding environments.

Table 2
EDX results of PRNF experiments (a) for DI water, NaCl, and seawater feeds (SMS sol-gel draw solution at pH 11), (b) multiple filtration cycles of PRNF membrane using seawater as feed (SMS sol-gel draw solution at pH 9) at 4 bar with cleaning for both the active and support layer.

a

	Active Layer (wt%)				Support layer (wt%)			
Elements	Pristine	DI water	NaCl	SW	Pristine	DI water	NaCl	SW
Oxygen	12.35	10.94	15.45	26.73	15.73	17.67	34.15	40.86
Carbon	71.29	65.82	47.26	19.49	77.14	74.32	26.91	12.47
Nitrogen	1.88	0	0	0	0	0	0	0
Silica	0	0.76	6.38	8.84	0	2.57	27.61	32.7
Calcium	0	0	0	1.99	0	0	0	0.39
Sodium	0	2.3	5.13	14.84	0	0.72	2.58	5.76
Sulphur	10.71	15.55	14.8	11.98	3.62	2.84	2.34	0
Magnesium	0	0	0	2.27	0	0	0	2.43
Chloride	0	0	6.54	9.67	0	0	1.63	1.33
Phosphorus	0	0	0	0	0.60	0.41	0.39	0
Iridium	3.41	4.52	4.44	4.19	2.55	2.45	4.39	4.07

To further investigate if the formed deposits matured during repeated operation cycles, XRD measurements were also conducted after one seawater cycle with SMS solution at pH 11 for both the active and support layers (in Supplementary Materials S6). The single-cycle XRD patterns showed the characteristic diffraction peaks of the membrane and exhibited only minor additional reflections when compared to the SMS powder reference. No strong or continuous crystalline scaling pattern was observed in a single filtration cycle of the membrane (Figure S3a, Supplementary Materials), indicating that inorganic deposition after a single FO cycle was minimal and localised, supporting that the detected scaling was not severe fouling and did not significantly alter the membrane structure. Overall, the XRD results suggest local/minor inorganic deposition rather than severe fouling or structural deterioration of the membrane. Therefore, Ca/silicate-associated deposition is discussed as a possible pathway, but Ca/Mg-silicate pore anchoring is not claimed as a confirmed mechanism without further chemical surface analysis.

SEM images of the pristine membrane show a clean and smooth active layer and a well-defined support layer (Figs. 4e-4j). For single filtration tests without cleaning, SEM images (Figs. 4g-4h) show a dense and consistent fouling layer on the active layer and partial pore blockage in the support layer, attributed to inorganic fouling consistent with silica gel. In contrast, the five-cycle filtration tests with NaOH cleaning (Figs. 4i-4j) show a significant removal of the fouling layer from the selective layer associated with pore reopening in the support layer, despite the trivial fouling residues on the membrane surface. The results confirm that fouling in the PRNF membrane with NaOH cleaning is mainly reversible and shifted from severe internal pore blocking to predominantly surface-associated deposits.

Generally, the fouling pathways at SMS sol-gel at pH 11 and pH 9 are completely different (Table 2a & 2b). At pH 11, silicate exists as monomeric SiO_3^{2-} and $HSiO_3^-$, which have a low tendency for polymerization. Initially, Ca reacts rapidly with SiO_3^{2-} to form crystalline/semicrystalline Ca-silicate nuclei that establish a heterogeneous nucleation on the membrane surface. Mg reaction with SiO_3^{2-} is slower due to its larger hydration shell, forming an amorphous Mg-silicate gel that deposits over the Ca-SiO_3^{2-} gel. At pH 9, silicate exists mainly as monosilicic acid, H_4SiO_4, with strong polymerization propensity even without Mg/Ca ions:

$$_nH_4SiO_4 \rightarrow (SiO_2)_n \cdot H_2O\ (gel) \quad (12)$$

.

As such, this would increase the silica-complexes residing on the membrane surface; however, the addition of EDTA to the seawater cycles was utilized to chelate the divalent ions such as Ca and Mg, which would reduce the likelihood of inorganic scaling. Mg will act as a crosslinker that interacts with polymeric silica to form a Mg-silicate gel complex, while Ca will act as a nucleation site, embedded in the gel matrix. A thick, compressible, amorphouss gel layer characterizes the fouling structure. Nevertheless, adding EDTA to the seawater feed sequesters Ca and Mg and, hence, hinders Mg-induced gel crosslinking at pH 9. The absence of fouling trigger, i.e., Mg and Ca, renders silica more scattered (monomeric/oligomeric) and less adhesive, resulting in a weak gel fouling that can be reversed by NaOH cleaning. The dominance of Si over Ca and Mg in the EDX analysis of the fouled membrane reflects that silica originates primarily from the SMS sol-gel draw solution rather than the seawater feed. Despite seawater containing substantially higher Ca (420 mg/L) and Mg (1311 mg/L) concentrations than dissolved silica (0.21 mg/L) (Supplementary Materials Table S1), the Si-rich sol-gel matrix drives silica deposition through reverse diffusion and concentration polarization at the membrane surface. As pH increases, silanol groups (Si-OH) become progressively deprotonated, promoting polymerization and the direct precipitation of amorphous silica onto the membrane, forming a persistent fouling layer. In contrast, Ca^{2+} and Mg^{2+} transport from the seawater feed side remains limited by the opposing concentration gradient, and their accumulation is further suppressed by EDTA complexation (logK ≈ 10.7 for Ca-EDTA; logK ≈ 8.7 for Mg-EDTA). FO membrane fouling studies using seawater feed consistently identify silica as the dominant inorganic foulant, with Ca and Mg detected as minor constituents of the fouling layer through EDX analysis [34,35]. At the same time, silica scaling caused by the polymerization of dissolved silica facilitates further deposition of biopolymers, while Ca and Mg contribute to secondary scaling effects. In FO-produced water studies, inorganic fouling included Ca, Mg, and chlorine, confirming their presence as trace co-foulants rather than dominant species, consistent with the trace levels observed in Table 2.

b

	Active Layer (wt%)		Support Layer (wt%)	
Elements	Pristine	After cleaning with NaOH	Pristine	After cleaning with NaOH
Oxygen	12.35	28.1	15.73	30
Carbon	71.29	61.0	77.14	57.5
Nitrogen	1.88	2.6	0	0
Calcium	0	0.8	0	0.9
Magnesium	0	3.7	0	1.9
Silica	0	2.7	0	8.5
Sodium	0	0.6	0	1.2
Sulphur	10.71	0	3.62	0
Chloride	0	0.4	0	0

.

Comparing the pristine PRNF membrane to the PRNF membrane after multiple filtration cycles, there was an increase in membrane thickness from 145 μm to 182.4 μm, approximately a 25.8% increase. Additionally, tensile and compression tests revealed an increase in Young's Modulus from 841.6 MPa for the pristine PRNF membrane to 996.04 MPa for the used one, while stiffness increased from 38,354 N/m for pristine PRNF to 50,590 N/m for the used one. The results show that cyclic filtration resulted in a denser and more mechanically stiff membrane structure due to increased surface depositions of foulants on the membrane.

FTIR analysis was undertaken on the PRNF membranes. The pristine PRNF membrane and the PRNF membrane with DI water as feed were compared and achieved similar peak ranges (Figs. 4c and 4d). The support layer for the pristine membrane at 3300 cm^{-1} signals a hydroxyl group, indicating that water molecules are readily available. A peak at around 2900 cm^{-1} indicates there are C-H stretching vibrations, suggesting CH_2 alkanes are present on the membrane. Between 1676 and 1710 cm^{-1}, a strong carbonyl stretching band of the polyamide layer was observed. The peaks between 1230 and 1244 cm^{-1} and 1490 cm^{-1} align with medium C-N stretching amine groups, while peaks between 1080 and 1114 cm^{-1} correspond to strong carbonyl stretching vinyl ether bonds. While within the fingerprint region (below 1500 cm^{-1}) aligns with C═H bending functional groups. Comparing the pristine membranes to the used membranes, it conveys the effects of feed ionic concentrations and their fouling efficacy on the membrane surface. The characterisations of the membrane when the feed was DI water and NaCl indicated that the fingerprint region was mostly retained with similar peaks across both the active and support layers. However, on the support layer, there were peaks in approximation to 570 cm^{-1}, which typically points to silicate group formation, corresponding with the draw solution's SMS sol-gel being in contact with the support layer.

However, there was a definite shift within the support layer, specifically with seawater as the feed, where new peaks formed between 567 and 594 cm^{-1}, suggesting greater deposition of inorganic material at that section. Looking at the PRNF cycles in particular, the active layer (Fig. 4d) shows broader groups across the graph. The active and support layers for the single seawater and PRNF cycles in the FTIR graph show them to be quite similar. The main changes for the active layer are around 1020 cm^{-1}, which shows Si-O silicones, 1523 cm^{-1} is an indication of strong N-O bands, which correlates with the EDX results, as nitrogen compounds have increased specifically in the PRNF cycles'

active layer. Additionally, this could forecast N-H bending associated with EDTA complexes that retain a residue on the membrane surface. At 1700 cm^{-1}, which is an indication of strong and stretching C═O carbonyl bands, relating to the presence of EDTA residue.

FTIR and XRD findings show that the main changes took place within the fingerprint region, which indicates localized inorganic surface deposits associated with silicate residues and salts. Together with EDX, surface elements detected such as Ca, Mg, Si, Na, and Cl, combined with XRD findings, these results indicate that fouling was mainly due to localized inorganic scaling dominated by calcite $CaCO_3$ with possible magnesium-based deposits. The existing experimental evidence from FTIR (Fig. 4d), SEM images (Figs. 4g–4j), and EDX data (Tables 2a and 2b) collectively supports the proposed pH-dependent fouling pathways. At pH 11, EDX Table 2a confirms coexistence of Ca (1.99 wt%) and Mg (2.27 wt%) on the active layer, consistent with rapid Ca-silicate nucleation followed by slower amorphous Mg-silicate gel overlayer deposition. EDX mapping of the seawater feed experiments from Table 2a has been added to the Supplementary Materials S6. FTIR (Fig. 4d) single-cycle SW test shows sharp Si-O-Si stretching bands indicative of crystalline or semicrystalline Ca-silicate structures, while SEM images (Figs. 4g–4h) reveal a dense, rigid fouling layer confirming structured Ca-silicate deposit morphology at pH 11. At pH 9, the five-cycle FTIR spectrum (Fig. 4d) shows broader Si-O-Si absorption bands consistent with amorphous Mg-crosslinked polymeric silica gel, while SEM images (Figs. 4i–4j) show significant fouling layer removal and pore reopening after NaOH cleaning, confirming the weaker and more reversible nature of the amorphous gel fouling at pH 9. EDX Table 2b further demonstrates a significant removal of Si (from 8.84% to 2.7% in the active layer) and Mg following EDTA and NaOH cleaning, confirming the reversibility of possible localized silicate species under the applied mitigation technique. While Ca ions are slightly higher in the PRNF cycles at pH 9, this can be due to the repetitive nature of the experiment and accumulation on the membrane surface. The cross-sectional SEM-EDX mapping (Supplementary Materials) and XRD of the membrane show limited and localized deposits. The cross-sectional SEM does not show a continuous fouling layer or structural damage to the membrane, and the EDX mapping shows weak and scattered inorganic signals. The XRD results indicate minor crystalline scaling deposits mainly in the form of calcite ($CaCO_3$), and minor brucite ($Mg(OH)_2$), with possible calcium silicate on the support layer of the membrane.

3.6. Implications and applicability

The SMS-based draw solutions are a nutritional sol-gel that provides water and essential nutrients, N and P, enabling agriculture in harsh environments and reducing water consumption. Combining FO with the sol-gel will further minimize stress on freshwater resources through direct seawater desalination, without the requirement of draw solution regeneration. PRNF membrane offers a considerable reduction in the cost of the membrane as well as better performance, represented by an outstanding increase in the water flux and RSF (Fig. 3). The membrane is commercially available at a competitive price compared to conventional FTSH_2O CTA FO membranes, offering more than 10 times cost savings [18].

In the FO process, the selection of an appropriate draw solution is critical, as it directly influences key performance factors including osmotic pressure, reverse salt flux (RSF), regeneration feasibility, and long-term operational stability (Table 3). Compared to some conventional draw solutions in the literature, SMS sol-gel has several advantages, such as high osmotic pressure, low RSF, easy to separate, and low cost [20]. Nevertheless, its major shortcomings are silica membrane fouling and elevated CP due to its viscous nature. NaCl, the most studied draw solution owing to its low cost, non-toxicity, and easy handling, has a major drawback, manifested by the energy-intensive regeneration cost [34]. In contrast, the application of divalent $MgSO_4$ draw solution was challenged by its low osmotic pressure and scaling problems [35]. Ionic liquids, another set of draw solutions, were reported in the FO process due to their tunable properties, but are unsuitable for commercial applications due to cost-ineffectiveness and complexity to regenerate [36]. Despite the novelty of fertilizer-based draw solutions to provide N and P for plants, nutrients leakage and imbalance are the major drawbacks [37]. This problem has been resolved in the SMS sol-gel, where nutrients are incorporated in the hydrogel network chain and are slowly released. Thermolytic draw solutions were widely studied, but their applications were limited because of ammonia leakage, contaminating the feed solution [38]. Similarly, organic draw solutions were scarcely used in the FO process due to promoting membrane fouling [35].

In comparison, the SMS sol-gel is cost-effective, eco-friendly, and enables easy physical separation. Its principal limitations include high viscosity and potential silica fouling. Nevertheless, SMS represents a promising and sustainable alternative to conventional draw solutions, particularly in applications demanding high water flux and minimal solute leakage.

While it can effectively capture divalent ions from the solution and minimize their complexation with silicate, EDTA slowly biodegrades and increases heavy metal mobility in the aquatic system if not properly managed. EDTA reduces the frequency of the membrane cleaning, prolongs the membrane life and stabilizes the water flux, but it increases the chemical costs. It should be used carefully to minimize its environmental impact.

Future studies should further explore membrane fouling characterization to focus on detailed crystalline analyses as a separate material

Table 3
Comparison of diverse draw solutions for seawater desalination by the FO process. The osmotic pressure was for a 1 M solution.

Draw solution	Dissociation factor (i)	Avg. osmotic pressure (atm)	Key advantages	Key drawbacks	Ref
NaCl	2	≈ 49 atm	Cheap, non-toxic, well-studied, easy handling, moderate osmotic pressure	Relatively high RSF needs high-energy RO for regeneration	[34]
$MgSO_4$	2 (effective often <2 due to ion pairing)	≈ 40–45 atm (depends on the dissociation)	Low RSF than monovalent solutions like NaCl, affordable, non-toxic	Low osmotic pressure, scaling risk, low diffusion, causing intensive CP	[35]
Ionic liquids	Variable (1–3 effective)	≈ 25–70 atm (depends on the type of IL)	Tuneable properties, low vapor pressure, low reverse salt flux	Not cost-effective, viscosity is high and hence the CP, regeneration complexity, and toxicity concerns	[36]
SMS sol-gel	2–3 (effective)	≈ 72 atm	Negligible RSF, easy physical separation, cost-effective, good water flux, and eco-friendly	High viscosity, CP, and silica fouling risk	[20]
Fertilizer draw solutions	2–3	≈ 50–75 atm (depends on the type of fertilizer solution)	No regeneration required, low cost, low RSF, high osmotic pressure	Nutrient leakage, limited applications, nutrient imbalance, and scaling problems.	[37]
Thermolytic draw solutions	2–3 (before decomposition)	≈ 49–73 atm	Reusable, regeneration at low temperature, and inexpensive	Ammonia leakage, odour, health and pollution problems, and corrosion concerns	[38]
Organic draw solutions	1	≈ 25 atm (depending on the type of organic solute)	Non-toxic, biodegradable, low RSF, tunable osmotic pressure	Low osmotic pressure, biofouling concerns, high viscosity and CP	[35]

investigation, utilizing advanced analytical methods such as TEM, RAMAN spectroscopy, XRD, and XPS. Furthermore, studies should conduct a pilot plant investigation to study the long-term process performance, fouling mitigation, cost breakdown, and industrial scalability. These parameters should be examined in a separate investigation.

4. Conclusion

FO experiments were carried out to demonstrate a distinct feature of the PRNF TS80 membrane using SMS sol-gel for seawater desalination. The practicality of using the SMS sol-draw solution is realized by applying the diluted sol-gel in agriculture to provide essential nutrients and growth stimulant agents to plants. The state-of-the-art PRNF TS80 membrane exhibited outstanding permselectivity and antifouling properties at a competitive cost to the conventional CTA FO membranes. After testing with three feed solutions, DI water, 0.5 M NaCl, and seawater, the PRNF water flux increased substantially with the applied pressure, recording 3.4, 2.8, and 1.8 times more water flux than the CTA in the FO experiments carried out with DI water, 0.5 M NaCl, and seawater, respectively. Experimental investigations also pinpointed the fouling drawback in the membrane filtration of SMS sol-gel, characterized by irreversible Mg/Ca silicates/carbonates that block the membrane's pores, forming a minor/localised fouling layer on the membrane surface. Fouling mitigation protocol successfully mitigated metal silicates fouling by sequestering Mg/Ca ions using EDTA, then cleaning the fouled membrane with NaOH at pH 11 to remove remaining silica fouling from the membrane surface. Fouling dropped by 18–142-fold by adding EDTA to the feed and NaOH cleaning. EDX, SEM, and XRD analysis suggested that fouling was mainly a localized inorganic deposition and/or scaling rather than a dense or continuous fouling layer. XRD analysis revealed that crystalline deposits were mainly associated with calcite, some brucite, and residual NaCl, while calcium silicate was also evident on the support layer. The EDX showed silicon content on the selective membrane layer reduced from 8.84% to 2.7% and on the support membrane layer from 32.7% to 8.5%, supporting the silicate associated depositions as a possible pathway but not as a severe and continuous fouling layer. The study findings evidently demonstrate the advantage of applying PRNF membranes in the FO process for improved water flux and reduced capital and running costs of the filtration process, making SMS sol-gel a viable draw solution for applications in hydrogel agriculture. Future research should concentrate on quantifying concentration polarization, systematically estimating net osmotic pressure gradients, analyzing pressure-corrected flux, reverse salt flux, and quantifying mass transfer to understand the decline in water flux in the PRNF membrane.

CRediT authorship contribution statement

Maryam Al-Ejji: Validation, Formal analysis, Data curation. **Hawari Alaa:** Validation, Formal analysis, Data curation. **Adnan Alhathal Alanezi:** Methodology, Formal analysis, Data curation. **Lilyan Alsaka:** Writing – review & editing, Writing – original draft, Validation, Formal analysis, Data curation. **Tayma Kazwini:** Writing – review & editing, Writing – original draft, Validation, Methodology, Investigation, Formal analysis, Data curation. **Ali Altaee:** Writing – review & editing, Writing – original draft, Validation, Resources, Methodology, Funding acquisition, Formal analysis, Data curation, Conceptualization. **Hossein Ali Khonakdar:** Validation, Investigation, Data curation. **Islam Md Rizwanul Fattah:** Validation, Supervision, Formal analysis, Data curation. **Zhaohua He:** Writing – review & editing, Writing – original draft, Investigation, Formal analysis. **Abdulmajeed Al Askar:** Validation, Formal analysis, Data curation. **Yahia Aedan:** Investigation, Formal analysis, Data curation.

Declaration of Competing Interest

The authors declare that they have no known competing financial interests or personal relationships that could have appeared to influence the work reported in this paper.

Acknowledgments

This research is made possible by a food security research award (MME03–1015–210003) from the Qatar National Research Fund (QNRF) in partnership with the Ministry of Municipality.

Appendix A. Supporting information

Supplementary data associated with this article can be found in the online version at doi:10.1016/j.jece.2026.123986.

Data availability

Data will be made available on request.

References

[1] F. Zheng, Y. Wang, Removal of antibiotics and antibiotic resistance genes by self-assembled nanofiltration membranes with tailored selectivity, J. Membr. Sci. 659 (2022) 120836, https://doi.org/10.1016/j.memsci.2022.120836.
[2] K. Banjerdteerakul, H. Peng, K. Li, COF-based nanofiltration membrane for effective treatment of wastewater containing pharmaceutical residues, J. Membr. Sci. 681 (2023) 121780, https://doi.org/10.1016/j.memsci.2023.121780.
[3] S. Zhao, L. Zou, C.Y. Tang, D. Mulcahy, Recent developments in forward osmosis: opportunities and challenges, J. Membr. Sci. 396 (2012) 1–21, https://doi.org/10.1016/j.memsci.2011.12.023.
[4] T.Y. Cath, A.E. Childress, M. Elimelech, Forward osmosis: principles, applications, and recent developments, J. Membr. Sci. 281 (2006) 70–87, https://doi.org/10.1016/j.memsci.2006.05.048.
[5] J.J. Huang, S. Chen, Y. Liao, Y. Chen, X. You, R. Wang, Performance, fouling and cleaning of a thin film composite hollow fiber membrane during fertiliser-drawn forward osmosis process for micro-polluted water, Environ. Sci. Water Res. Technol. 7 (2021) 1279–1291, https://doi.org/10.1039/D0EW00996B.
[6] B. Corzo, T. de la Torre, C. Sans, R. Escorihuela, S. Navea, J.J. Malfeito, Long-term evaluation of a forward osmosis-nanofiltration demonstration plant for wastewater reuse in agriculture, Chem. Eng. J. 338 (2018) 383–391, https://doi.org/10.1016/j.cej.2018.01.042.
[7] I. Ibrar, A. Altaee, J.L. Zhou, O. Naji, D. Khanafer, Challenges and potentials of forward osmosis process in the treatment of wastewater, Crit. Rev. Environ. Sci. Technol. 50 (2020) 1339–1383, https://doi.org/10.1080/10643389.2019.1657762.
[8] J.R. McCutcheon, M. Elimelech, Influence of concentrative and dilutive internal concentration polarization on flux behavior in forward osmosis, J. Membr. Sci. 284 (2006) 237–247, https://doi.org/10.1016/j.memsci.2006.07.049.
[9] G. Blandin, A.R.D. Verliefde, C.Y. Tang, A.E. Childress, P. Le-Clech, Validation of assisted forward osmosis (AFO) process: Impact of hydraulic pressure, J. Membr. Sci. 447 (2013) 1–11, https://doi.org/10.1016/j.memsci.2013.06.002.
[10] B. Kim, G. Gwak, S. Hong, Analysis of enhancing water flux and reducing reverse solute flux in pressure assisted forward osmosis process, Desalination 421 (2017) 61–71, https://doi.org/10.1016/j.desal.2017.04.007.
[11] S. Jamil, S. Jeong, S. Vigneswaran, Application of pressure assisted forward osmosis for water purification and reuse of reverse osmosis concentrate from a water reclamation plant, Sep. Purif. Technol. 171 (2016) 182–190, https://doi.org/10.1016/j.seppur.2016.07.036.
[12] J. Peng, X. Zhao, Y. Su, H. Wu, Z. Jiang, Stimuli Responsive, in: E. Drioli, L. Giorno (Eds.), Encyclopedia of Membranes, Springer Berlin Heidelberg, Berlin, Heidelberg, 2016, pp. 1826–1827.
[13] R. Ou, Y. Wang, H. Wang, T. Xu, Thermo-sensitive polyelectrolytes as draw solutions in forward osmosis process, Desalination 318 (2013) 48–55, https://doi.org/10.1016/j.desal.2013.03.022.
[14] J. Zeng, S. Cui, Q. Wang, R. Chen, Multi-layer temperature-responsive hydrogel for forward-osmosis desalination with high permeable flux and fast water release, Desalination 459 (2019) 105–113, https://doi.org/10.1016/j.desal.2019.02.002.
[15] D. Khanafer, A. Altaee, A.H. Hawari, J. Zhou, L. Alsaka, Innovative stimuli-responsive membrane MSF brine rejection dilution by tertiary treated sewage effluent, J. Environ. Manag. 365 (2024) 121517, https://doi.org/10.1016/j.jenvman.2024.121517.
[16] D. Ahmed, H. Isawi, N. Badway, A. Elbayaa, H. Shawky, Highly porous cellulosic nanocomposite membranes with enhanced performance for forward osmosis desalination, Iran. Polym. J. 30 (2021) 423–444, https://doi.org/10.1007/s13726-021-00901-4.
[17] A. Altaee, D. Khanafer, A. Hawari, in, Method. Appar. Syst. Seawater Treat. (2023).

[18] D. Khanafer, A. Altaee, A.H. Hawari, Y. Aedan, J. Zhou, A.K. Samal, Seawater pretreatment for thermal plant by pressure stimuli-responsive forward osmosis membrane, Energy Nexus 19 (2025) 100488, https://doi.org/10.1016/j.nexus.2025.100488.
[19] Y. Aedan, A. Altaee, J.L. Zhou, H.K. Shon, Perfluorooctanoic acid-contaminated wastewater treatment by forward osmosis: Performance analysis, Sci. Total. Environ. 934 (2024) 173368, https://doi.org/10.1016/j.scitotenv.2024.173368.
[20] T. Kazwini, A. Altaee, I. Ibrar, F. Alkadour, A.H. Hawari, J. Zhou, L. Alsaka, Sodium metasilicate sol-gel draw solution for seawater desalination and supplementing nutrients to soil, Desalination 600 (2025) 118517, https://doi.org/10.1016/j.desal.2024.118517.
[21] T. Kazwini, A. Altaee, L. Alsaka, A. Hawari, E. Warmbier, H. Shon, S. Yadav, A. K. Samal, J. Zhou, Y. Aedan, Fouling mitigation for cellulose triacetate and thin-film composite forward osmosis membranes for seawater desalination by sodium metasilicate sol-gel, Sci. Total. Environ. 1001 (2025) 180525, https://doi.org/10.1016/j.scitotenv.2025.180525.
[22] R. Shivappa, B. J, B. Ms, P. Sr, U. K, M. A, P. Pati, S.D. Mohapatra, G.-P.-P. Govindharaj, Dual Role of Potassium Silicate and Salicylic Acid: Plant Growth Promotor and Plant Immunity Booster Against Bakanae Disease of Rice, Silicon 16 (2024) 1173–1182, https://doi.org/10.1007/s12633-023-02738-3.
[23] S.A. Greenberg, D. Sinclair, Polym. silicic Acid. 59 (1955) 435–440.
[24] Y. Aedan, A. Altaee, H.K. Shon, Performance of pressure stimuli-responsive nanofiltration and cellulose acetate forward osmosis membranes for PFOA contaminated wastewater treatment, Sep. Purif. Technol. 364 (2025) 132458, https://doi.org/10.1016/j.seppur.2025.132458.
[25] D. Khanafer, S. Yadav, N. Ganbat, A. Altaee, J. Zhou, A.H. Hawari, Performance of the pressure assisted forward osmosis-msf hybrid desalination plant, Water 13 (2021) 1245, https://doi.org/10.3390/w13091245.
[26] H.E. Bergna, Colloid Chemistry of Silica, in: The Colloid Chemistry of Silica, American Chemical Society, 1994, pp. 1–47.
[27] N.A. Pham, D.Y.F. Ng, K. Goh, Z. Dong, R. Wang, Assessing the potential of integrally skinned asymmetric hollow fiber membranes for addressing membrane fouling in pressure retarded osmosis process, Desalination 520 (2021) 115347, https://doi.org/10.1016/j.desal.2021.115347.
[28] C.Y. Tang, Q. She, W.C.L. Lay, R. Wang, A.G. Fane, Coupled effects of internal concentration polarization and fouling on flux behavior of forward osmosis membranes during humic acid filtration, J. Membr. Sci. 354 (2010) 123–133, https://doi.org/10.1016/j.memsci.2010.02.059.
[29] Y. Chun, D. Mulcahy, L. Zou, I. Kim, A short review of membrane fouling in forward osmosis processes, Membranes 7 (2017) 30, https://doi.org/10.3390/membranes7020030.
[30] G.T. Gray, J.R. McCutcheon, M. Elimelech, Internal concentration polarization in forward osmosis: role of membrane orientation, Desalination 197 (2006) 1–8, https://doi.org/10.1016/j.desal.2006.02.003.
[31] A. Tiraferri, N.Y. Yip, A.P. Straub, S. Romero-Vargas Castrillon, M. Elimelech, A method for the simultaneous determination of transport and structural parameters of forward osmosis membranes, J. Membr. Sci. 444 (2013) 523–538, https://doi.org/10.1016/j.memsci.2013.05.023.
[32] A. Altaee, G. Zaragoza, G.J. Millar, A.O. Sharif, A.A. Alanezi, Limitations of osmotic gradient resource and hydraulic pressure on the efficiency of dual stage PRO process, Desalin. Water Treat. 105 (2018) 11–22, https://doi.org/10.5004/dwt.2018.22128.
[33] J. Fei, Y. Lyu, X. Zhong, D.E. Wiley, Z. Liu, Q. She, Calcium phosphate scaling in osmotically driven membrane processes: limiting flux behavior and its implications for scaling mitigation, J. Membr. Sci. 631 (2021) 119351, https://doi.org/10.1016/j.memsci.2021.119351.
[34] Y. Xu, Y. Zhu, Z. Chen, J. Zhu, G. Chen, A comprehensive review on forward osmosis water treatment: recent advances and prospects of membranes and draw solutes, Int. J. Environ. Res. Public. Health 19 (2022) 8215, https://doi.org/10.3390/ijerph19138215.
[35] M. Hamdan, A.O. Sharif, G. Derwish, S. Al-Aibi, A. Altaee, Draw solutions for Forward Osmosis process: osmotic pressure of binary and ternary aqueous solutions of magnesium chloride, sodium chloride, sucrose and maltose, J. Food Eng. 155 (2015) 10–15, https://doi.org/10.1016/j.jfoodeng.2015.01.010.
[36] M.A.M. Abdullah, M.S. Man, S.B. Abdullah, S.M. Saufi, A glance on thermo-responsive ionic liquids as draw solution in forward osmosis system, Desalin. Water Treat. 206 (2020) 165–176, https://doi.org/10.5004/dwt.2020.26317.
[37] M. Gulied, F. Al Momani, M. Khraisheh, R. Bhosale, A. AlNouss, Influence of draw solution type and properties on the performance of forward osmosis process: energy consumption and sustainable water reuse, Chemosphere 233 (2019) 234–244, https://doi.org/10.1016/j.chemosphere.2019.05.241.
[38] H. Luo, Q. Wang, T.C. Zhang, T. Tao, A. Zhou, L. Chen, X. Bie, A review on the recovery methods of draw solutes in forward osmosis, J. Water Process. Eng. 4 (2014) 212–223, https://doi.org/10.1016/j.jwpe.2014.10.006.